Journal of Molecular Liquids 437 (2025) 128687

Contents lists available at ScienceDirect

Journal of Molecular Liquids

journal homepage: www.elsevier.com/locate/molliq

# Molecular dynamics underlying the regulation of a gas hydrate by amylose

Jaeyoung Kim [a], Seyong Choi [a], Kiduk Kim [a], Sungwook Chung [b,c,d], Joonkyung Jang [a,*]

[a] Department of Nanoenergy Engineering, Pusan National University, Busan 46241, Republic of Korea
[b] School of Chemical Engineering, Pusan National University, Busan 46241, Republic of Korea
[c] School of Chemical and Biomolecular Engineering, Pusan National University, Busan 46241, Republic of Korea
[d] Institute of Environment & Energy, Pusan National University, Busan 46241, Republic of Korea

ARTICLE INFO

*Keywords:*
Gas hydrate
Molecular dynamics simulation
Amylose
Methane

ABSTRACT

When mixed with a gas under a high pressure, a liquid water forms crystalline cavities that can host gas molecules. The resulting gas hydrate can be an important energy resource but also causes a blockage of a pipeline in the ocean. Given regulation of a gas hydrate is often desired, starch has been considered as a biodegradable inhibitor of a gas hydrate. Currently, the molecular mechanism behind the regulation is not fully understood. By using all-atom molecular dynamics simulation, we examine whether and how an amylose (main component of starch) additive regulates a methane hydrate at the molecule level. For comparison, a 2,3,6-*O*-methyl-amylose (OMet-amylose) additive, which is bulkier but has fewer hydroxyl groups, was also investigated. The amylose additive regulates a methane hydrate through two mechanisms: steric hindrance and hydrogen bonding interaction with a seed of hydrate. The hydroxyl groups of the amylose make ring structures which hamper the formation of a hydrate cage. The OMet-amylose however does not form such a ring structure, giving a weaker inhibition than the amylose. The present molecular insights offer guidelines for designing biodegradable additives based on natural starch.

## 1. Introduction

*Gas hydrates*, such as the methane hydrates naturally formed in the bottom of ocean, are crystalline water with cavities (or cages) that can host gaseous molecules such as methane, ethane and carbon dioxide molecules [1–3]. Gas hydrates are mainly composed of five types of cavities: $5^{12}$, $5^{12}6^2$, $5^{12}6^4$, $5^{12}6^8$ and $4^35^66^3$ cavities, where 4, 5 and 6, respectively, represent the rings of four, five and six water molecules, and the superscripts designate numbers of such rings in a cavity. The structure of a gas hydrate is determined by how these cavities are interconnected via the H bond network of water molecules. Depending on the species of gas, a gas hydrate takes one of three structures: structure I (sI) comprises $5^{12}$ and $5^{12}6^2$ cages; structure II (sII) $5^{12}$ and $5^{12}6^4$ cages; structure H (sH) contains $5^{12}$, $4^35^66^3$ and $5^{12}6^8$ cages [2]. Gas hydrates find various potential applications, including an energy resource, sewage treatment, seawater desalination, carbon dioxide sequestration, gas storage and gas separation [4–9]. The stability of a gas hydrate under a given thermodynamic condition depends on the identity of gas. Therefore, a gas hydrate can be used for selective separation of gas mixtures, such as the separation of methane from coal mine gases of methane, nitrogen, and oxygen [10–12]. Global reserves of gas hydrates are estimated to exceed by far those of conventional natural gas, and therefore can serve as energy resources and sustainable supplies [13–15]. Moreover, the selectivity of a gas hydrate makes it suitable for a gas separation process which is industrially important [2,16,17].

On the other hand, gas hydrates cause blockages of oil or gas pipelines in ocean [18,19]. In such cases, chemical *additives* are injected to regulate the formation of a gas hydrate. These additives, called hydrate inhibitors or anti-agglomerants, can be classified into *thermal hydrate inhibitors* (THIs) and *kinetic hydrate inhibitors* (KHIs). The THIs, such as mono-ethylene glycol, methanol, and diethylene glycol, shift the thermodynamic condition of a gas hydrate toward a lower temperature and higher pressure region, thereby inhibiting a thermodynamically stable gas hydrate [20,21]. However, the THIs must be used with high doses (20–50 wt%), causing high costs and pollutions [18,20]. The KHIs do not affect the thermodynamics conditions of gas hydrates but kinetically retard the nucleation of a gas hydrate [22,23]. The water-soluble polymers, such as polyvinylpyrrolidone and polyvinylcaprolactam, have been used as KHIs. The KHIs also raise environmental concerns because of their poor biodegradabilities [21,24,25].

Natural polysaccharides (e.g., cellulose, starch, guar, and xanthan gum) are biodegradable, non-toxic, and widely available, and therefore

* Corresponding author.
*E-mail address:* jkjang@pusan.ac.kr (J. Jang).

https://doi.org/10.1016/j.molliq.2025.128687
Received 31 July 2025; Received in revised form 13 September 2025; Accepted 4 October 2025
Available online 6 October 2025

have been considered as candidates for KHIs [22,26–29]. Among these, several groups have investigated the kinetic inhibitory effects of starch on a gas hydrate [22,29,30]. Various types of starch (tapioca, cassava, and cationic starches) have shown to regulate the growth of a gas hydrate. With a further addition of polyoxides, these starches exhibited even more suppression of gas hydrates. On the contrary, the potato and maize starches have been reported to *promote* the growth of a methane hydrate [31,32], as much as sodium dodecyl sulfate (SDS), a common promoter of a gas hydrate.

Currently, whether and how starch inhibits a gas hydrate remains unclear especially at the molecular level. Over the years, *molecular dynamics* (MD) simulation has been utilized to study various inhibitors of gas hydrates. Go et al. investigated the regulatory effects of dipeptides ($_L$-alanyl-$_L$-alanine, $_L$-alanyl-glycine, and glycylglycine) on a methane hydrate [33]. The N-termini of each dipeptide formed *hydrogen* (H) bonds with water molecules, thereby preventing the growth of a hydrate. Inhibition of a methane hydrate with the additive of lignin or pectin has been studied [34,35]. Both the lignin and pectin additives inhibited methane hydrates by reducing the transfer of methane to water and by forming the abnormal (non-hydrate) cages with water molecules. Zhang et al. and Maddah et al. studied the influence of an antifreeze protein (AFP) on a gas hydrate [36,37]. The hydrophobic and hydrophilic residues of AFP synergistically adsorbed onto the surface of hydrate, and the shape of side chain was in important the regulation of a hydrate.

Herein, we report an extensive all-atom MD simulation on a methane hydrate growing in the presence of an amylose additive. Amylose, along with amylopectin, mainly constitutes starch and is a linear polymer which is linked by 1 → 4-α-glycosidic bonds [38,39]. We are unaware of any molecular simulation study on the role of amylose as an inhibitor of a gas hydrate. The present study addresses the contentious issue of whether starch inhibits or promotes a gas hydrate. We provide the molecular-level insights into such regulatory effects of starch which are not available in experiments. For comparison, 2,3,6-tri-*O*-methyl-amylose (OMet-amylose) which is bulkier than amylose but has less hydroxyl groups available for H bonds was also studied. We uncover the molecular insights into the inhibitory mechanism of amylose on the growth of a gas hydrate. Amylose indeed regulates a methane hydrate, more strongly than OMet-amylose additive. The H bond interaction, rather than a steric hindrance, is identified as the main mechanism of the regulation by the amylose additive. By providing the molecular details unavailable by experiment means, the present study fills in the gap in our understanding of the inhibition of a gas hydrate by starch. This work also aims to provide molecular guides in designing an effective and biodegradable additive for controlling gas hydrates.

## 2. Simulation methods

The present amylose additive molecule has a degree of polymer (DP) of 10 (Fig. 1a). We additionally modeled an OMet-amylose molecule in which the hydroxyl groups at positions 2, 3, and 6 of the amylose molecule was replaced by methoxy groups (Fig. 1b). The growth of a methane hydrate was emulated by introducing a *nucleation seed* modeled as a 6 × 2 × 1 supercell of the *sI* unit cell of hydrate [40]. On top of the

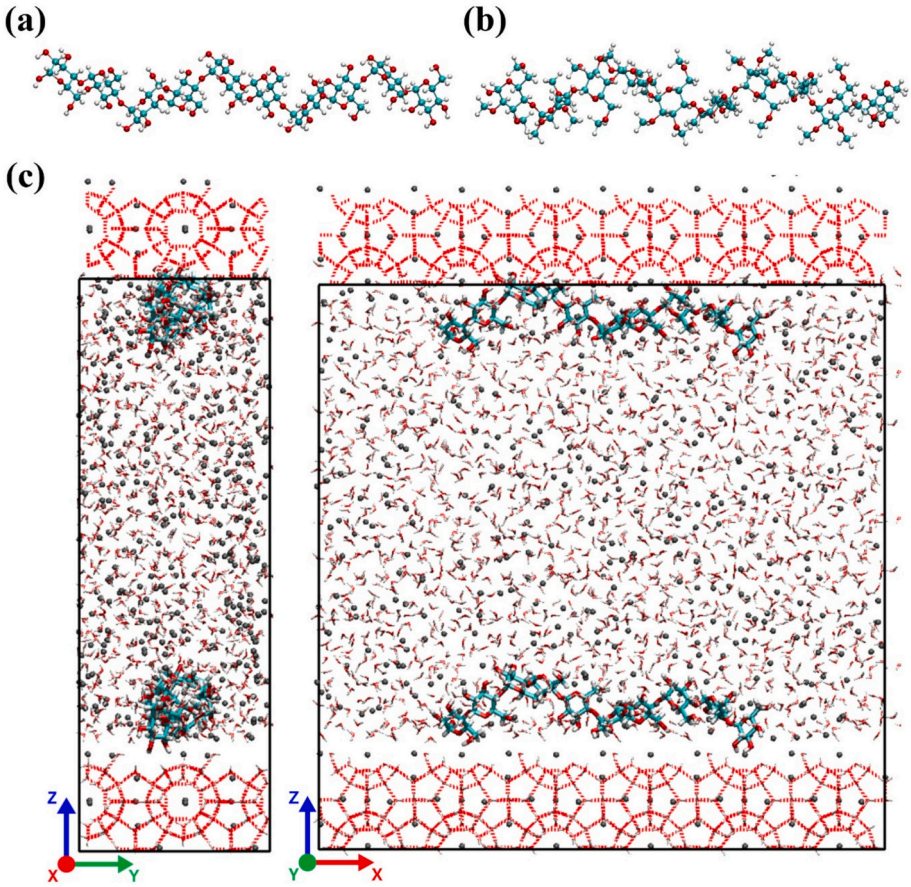


**Fig. 1.** Amylose (a) and OMet-amylose (b) molecules simulated in the present simulation. (c) Initial set up for the MD simulation of the growth of a methane hydrate. An (OMet-) amylose molecule is placed above the seed of a methane hydrate (with the sI structure) located at the bottom. Due to the PBCs of simulation, the seed of hydrate also exists at the top of the simulation box. We added another (OMet) amylose molecule near the top of simulation box. The H bonds between water molecules of the seed are drawn as red-dotted lines. Methane molecules are uniformly dispersed in the liquid water above the seed. (For interpretation of the references to colour in this figure legend, the reader is referred to the web version of this article.)

seed, 384 methane and 2208 water molecules were added (Fig. 1c). The amylose or OMet-amylose molecules were placed near the seed (as shown in Fig. 1c). For equilibration, a 0.5 ns-long MD simulation was run under an NPT condition. We then executed a 1-μs-long MD simulation for production of data at 250 K and 100 bar (NPT condition).The present condition of 250 K and 100 bar is frequently used in the research of gas hydrate. A gas hydrate readily forms at this low temperature and high pressure, which makes it a good condition for studying the inhibition of gas hydrate with an additive. The present temperature and pressure corresponded to the hexagonal ice region of the phase diagram for TIP4P/Ice water model [41]. The particle-mesh-Ewald (PME) method was used to include the long-ranged electrostatic interactions [42]. The Newtonian equation of motion was propagated in time with the leapfrog integrator with a time step of 2.0 fs [43]. The Lennard-Jones and short-ranged Coulomb interactions were both cut off at 1.0 nm. The linear constraint solver (LINCS) algorithm was employed to constrain the bonds involving H atoms [44]. The *periodic boundary conditions* (PBCs) was applied in all three directions. The Nose-Hoover thermostat and the Parrinello-Rahman barostat were used with the time constants of 1 and 2 ps, respectively, for the temperature and pressure coupling [45–47]. We used the force fields of GLYCAM06j, OPLS/AA, and TIP4P/Ice, respectively, to describe the (OMet-) amylose, methane, and water molecules, respectively [41,48–50]. The initial structures of the amylose and OMet-amylose molecules were generated by employing Chemistry at Harvard Macromolecular Mechanics-Graphical User Interface (CHARMM-GUI). All the MD simulation methods were implemented by using Gromacs software [51–54].

We followed the potential energy of the system and the number of hydrate cages during the 1 μs-long MD simulation. The hierarchical topology ring (HTR) algorithm was used to count the number of cages [55]. We also tracked down the *F4 order parameter* defined as $F_4 = <\cos 3\varphi>$, where φ is the H-O…O-H dihedral angle between two arbitrary water molecules. Note $F_4$ is about 0.7 and −0.04 for the sI hydrate and liquid water, respectively [56]. Therefore, an increase in $F_4$ reflects the growth of a hydrate.

We also followed the *mean-square displacements* (MSDs) of water and methane molecules, defined as $\boldsymbol{MSD_i} = \langle \|\boldsymbol{r_i}(t) - \boldsymbol{r_i}(t_0)\|^2 \rangle$, where $t$ and $\boldsymbol{r_i}(t)$ represent time and the position vector of the $i$th molecule at time t, respectively. The MSD of each molecule was defined as the mass-weighted average of the displacements of constituting atoms. The *radial distribution functions* (RDFs) for the oxygen atoms of water and for carbon atoms of methane were calculated. The RDF for the pair of atoms $j$ and $i$ was defined as $\boldsymbol{g_{i-j}}(\boldsymbol{r}) = \left(1/4\pi\rho_j r^2\right)\left(dN_{i-j}/dr\right)$, where $\rho_j$ and $dN_{i-j}$ are the average density of atom $j$ and the average number of atom $j$ around atom $i$ in the range of $r \sim r + dr$. The RDFs were calculated by using the final (0.950–1.000 μs) portion of MD simulation. In addition, the number of H bonds made between the (OMet-) amylose and water molecules were checked. The *solvent accessible surface area* (SASA) was calculated to estimate the steric effects of the (OMet-) amylose molecule. We used the visual molecular dynamics (VMD) software to visualize and

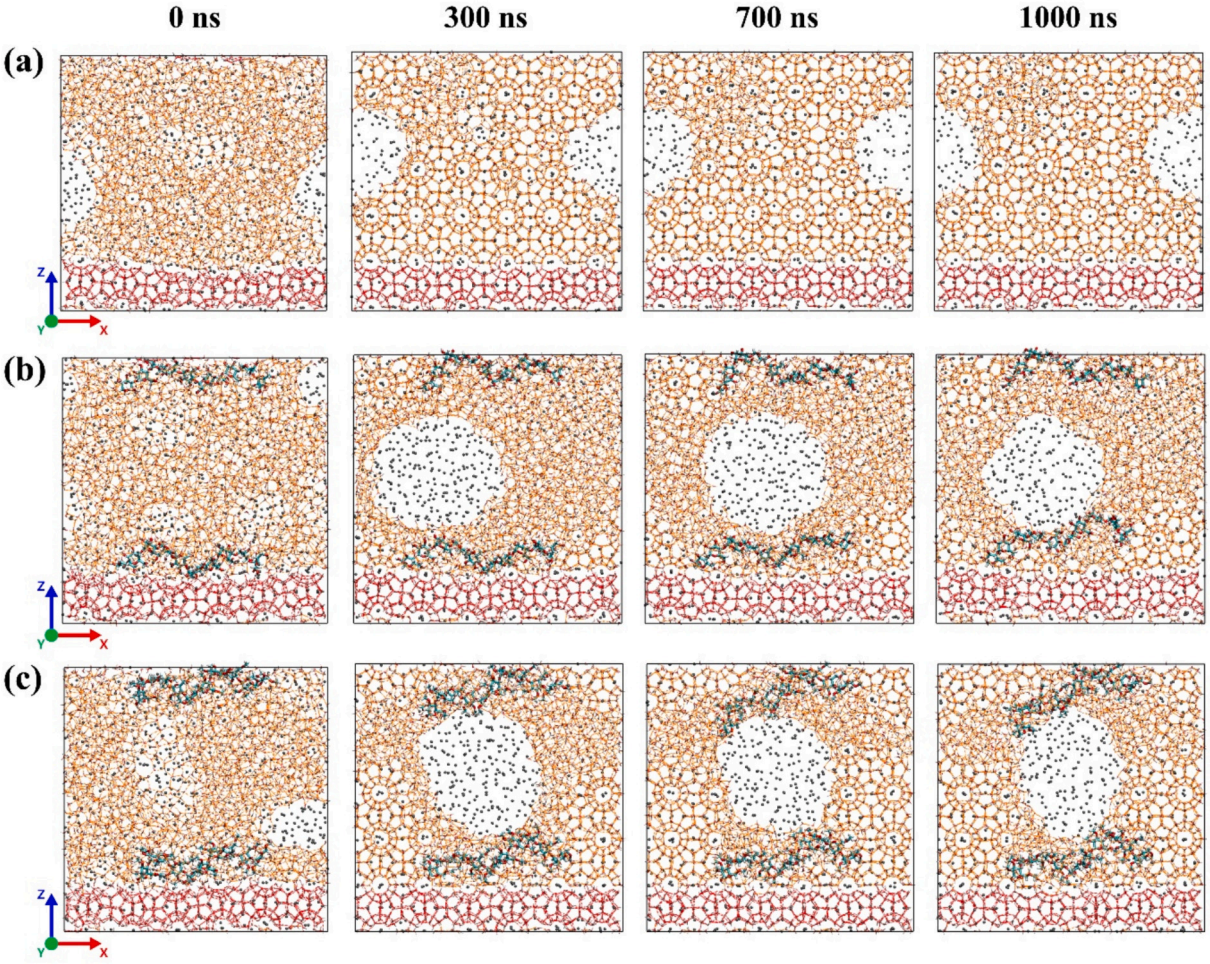


**Fig. 2.** Growth of a methane hydrate without any additive (a), with the amylose additive (b), and with the OMet-amylose additive (c). We illustrate the simulation snapshots taken at 0, 300, 700, and 1000 ns (from left to right). The additive and methane molecules are drawn as licorices and gray spheres, respectively. Shown in red and orange dotted lines are the H bonds of water molecules belonging to the seed and liquid water, respectively. (For interpretation of the references to colour in this figure legend, the reader is referred to the web version of this article.)

analyze the MD simulation snapshots [57]. All the results were obtained by averaging over two independent MD trajectories. Two independent simulations gave virtually identical results.

## 3. Results and discussion

In Fig. 2, we illustrate the growth of a methane hydrate for the cases without any additive (Fig. 2a) and with the amylose (Fig. 2b) and OMet-amylose (Fig. 2c) additive molecules. Without an additive (Fig. 2a), the liquid water molecules largely joined the growing hydrate within 300 ns. In the presence of the amylose molecule however, (Fig. 2b), the hydrate barely grew in time, and the liquid water molecules predominantly remained liquid, even at 1000 ns. Within 300 ns, the methane molecules, initially dispersed in the liquid water, aggregated to form a single large bubble. The seed of hydrate slightly grew in time, mainly in the region not in contact with the amylose molecule. Presumably, the amylose molecule sterically hindered the liquid water molecules from approaching and contacting the seed. This steric hindrance, however, was not solely responsible for the regulation by amylose. When the bulkier OMet-amylose molecule was added (Fig. 2c), the hydrate grew faster than with the amylose molecule. Most of the liquid water molecules participated in the hydrate cages of methane within 1 μs. By 300 ns, the methane molecules aggregated to form a single large bubble. Compared to the case without any additive, the OMet-amylose additive somewhat slowed down the growth of a hydrate.

We investigate the molecular details behind the regulation of a hydrate by the (OMet-) amylose additive. Fig. 3 illustrates the change in the first hydration shell surrounding the (OMet-) amylose molecule, taken from the initial portion of MD simulation (50–100 ns). The amylose molecule steadily maintained the H-bonds with the water molecules of the seed. The water molecules of the hydration shell contacting the seed below were nearly unchanged in identity with time, signifying the stable adsorption of the amylose molecule to the seed. In contrast, the water molecules of the hydration shell contacting the liquid water considerably changed over time. In short, the amylose molecule firmly adsorbed to the water molecules of the seed but substantially perturbed the surrounding liquid water molecules. The perturbed liquid water molecules should be more fluidic and less tend to form a solid-like hydrate structure. Also, as shown in Fig. 4, the hydroxyl groups of the amylose molecule developed stable ring structures with water molecules of the seed. These ring structures also hampered the formation of hydrate cages that can capture methane molecules.

The OMet-amylose molecule made a secure contact with the seed of hydrate through H bonds much less in number than the amylose molecule (Fig. 5). The hydration shell around OMet-amylose molecule however did not change much with time. The OMet-amylose molecule maintained a stable hydration shell near the seed through the H bonds. Also, the hydration shell in contact with the liquid water did no change much, unlike that of the amylose molecule. Consequently, the OMet-amylose molecule did not perturb the liquid water as much as the amylose molecule. In this case, the liquid water should be more like the one without any additive. Consequently, the regulation of the hydrate by the OMet-amylose molecule should be weaker than by the amylose molecule. In addition, we did not observe any ring structures found with the amylose molecule as an additive. Similar behaviors of the hydration shells of the amylose and OMet-amylose molecules were observed in the final portion of MD simulation (950–1000 ns) (Figs. S1 and S2).

In order to study the molecular dynamics behind the growth of a hydrate, we followed the time evolutions of the potential energy of system, the number of hydrate cages, and $F_4$ parameter (Fig. 6). In the absence of the (OMet-) amylose additive, the potential energy decreased and converged after 350 ns. In the presence of the amylose or OMet-amylose additive however, the potential energy slowly decreased without convergence even at 1000 ns.

Fig. 6b illustrates how many hydrate cages ($5^{12}$, $5^{12}6^2$, $5^{12}6^3$ or $5^{12}6^4$ type) are formed over the time of simulation. Without an additive, the number of cages increased and converged to approximately 400 at 350 ns. By contrast, the number of cages with the (OMet-) amylose additive slowly rose and did not converge within 1 μs. The number of cages was smaller than with the amylose additive, signifying the stronger regulation of hydrate by the amylose additive.

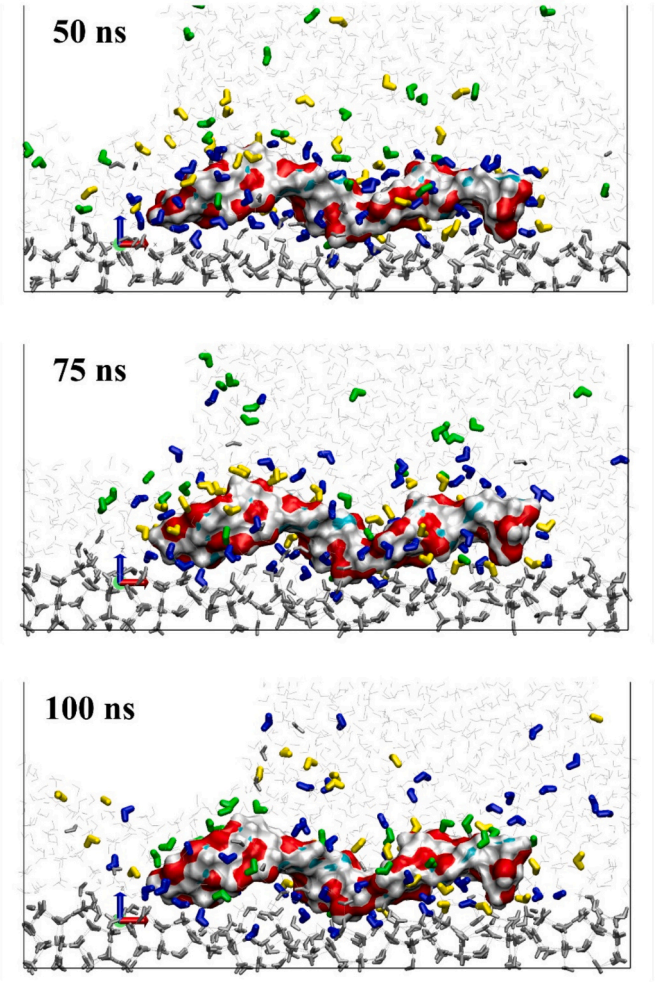


**Fig. 3.** Amylose molecule (drawn as a solid surface) interacting with the seed of a methane hydrate below (shown in gray). The water molecules belonging to the first hydration shell of the amylose molecule at 50, 75, and 100 ns are depicted in blue, yellow, and green, respectively. (For interpretation of the references to colour in this figure legend, the reader is referred to the web version of this article.)

As shown in Fig. 6c, the initial F4 value was ~0.1 for all the cases, because both the hydrate seed and liquid water were present. In the absence of an additive, F4 quickly increased and leveled off to 0.65 after 350 ns. This indicates that the most water molecules participated in the growing hydrate. With the amylose or OMet-amylose additive, F4 parameter grew rather slowly. The increase in F4 was slowest with the amylose additive, again indicating that the amylose additive most strongly inhibited the growth of hydrate. $F_4$ is an order parameter indicative of the phase transition from the liquid to hydrate, increasing from −0.04 to 0.7 as the phase of water changes from a liquid to hydrate [56]. However, $F_4$ does not have a quantitative (e.g., linear) correlation with the growth rate of a hydrate.

In Fig. 7, the MSDs of water (a) and methane (b) molecules are plotted vs. time. Without an additive, the MSD of water most slowly grew in time. The slope of MSD with respect to time changed from $5.85 \times 10^{-8}$ to $3.90 \times 10^{-7}$ $cm^2/s$ near 800 ns. Here, the water molecules were almost frozen because their participation in the growing gas hydrate. By contrast, with the amylose or OMet-amylose additive, the MSD

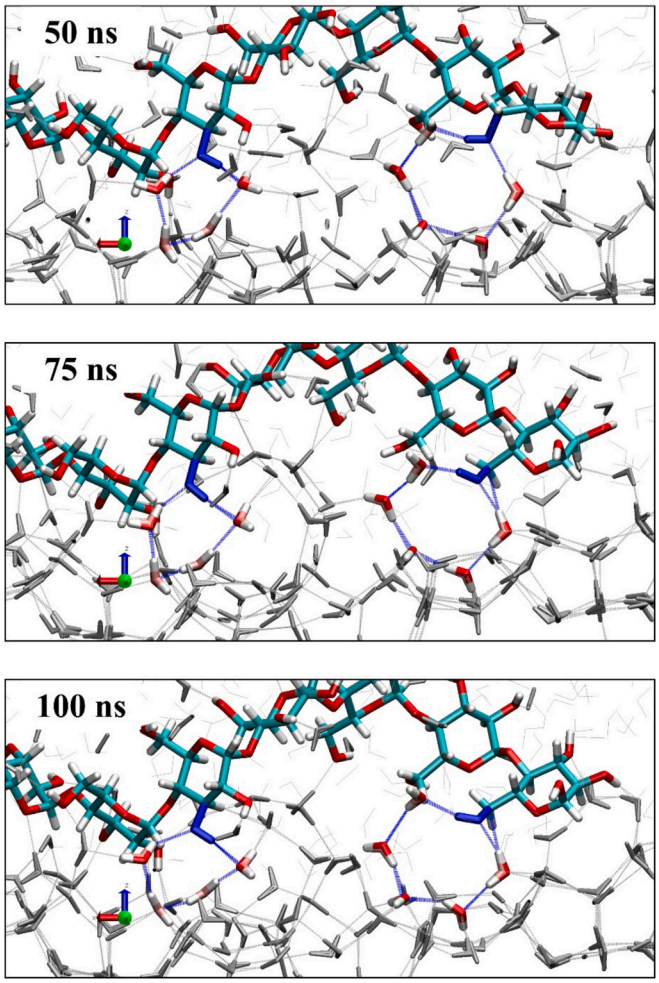


**Fig. 4.** Ring structures hampering the growth of a hydrate with the amylose molecule. The amylose and water molecules are drawn as licorices. Shown in blue are the hydroxyl groups of the amylose molecule which make two ring structures with the water molecules belonging to the hydrate seed below. (For interpretation of the references to colour in this figure legend, the reader is referred to the web version of this article.)

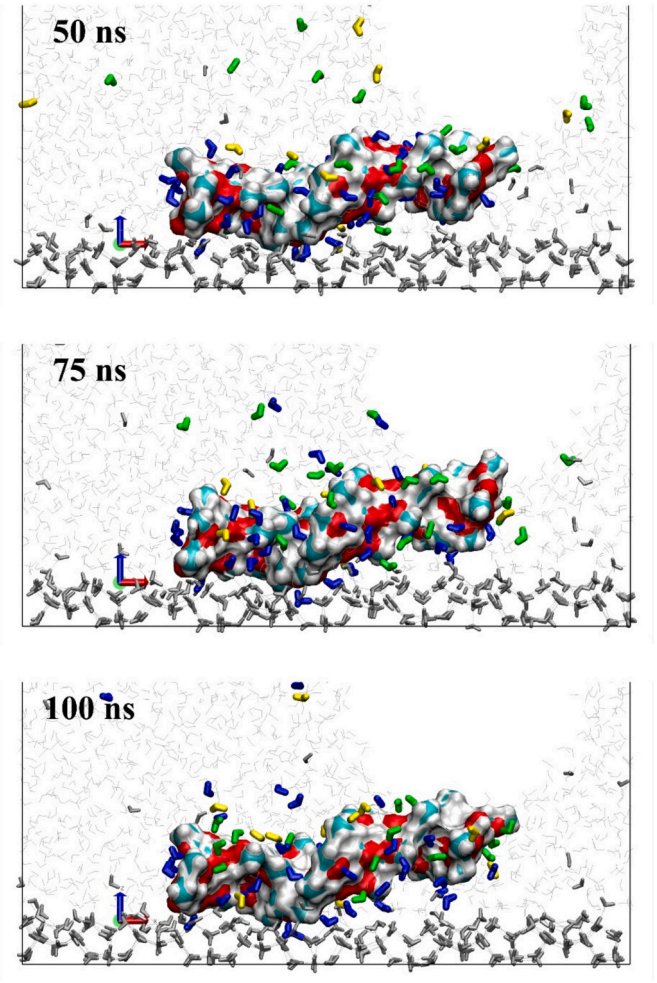


**Fig. 5.** OMet-amylose molecule (drawn as a solid surface) interacting with the seed of a methane hydrate below (shown in gray). The water molecules belonging to the first hydration shell of the OMet-amylose molecule at 50, 75, and 100 ns are depicted in blue, yellow, and green, respectively. (For interpretation of the references to colour in this figure legend, the reader is referred to the web version of this article.)

of water relatively rapidly and linearly increased with time. This signified the initially liquid water molecules remained liquid with the (OMet-) amylose additive. Regardless of the presence of additive, the MSD of water grew in time at least 3 times slower than that of the bulk water predicted by using the diffusion coefficient ($=1.70 \times 10^{-6}$ $cm^2/s$) calculated at 245 K and 1000 bar [58]. The slow diffusion of the present liquid water originated from the presence of methane and the seed in the system.

The MSD of methane molecules without additive slowly rose with time because most of methane molecules became trapped in the cavities of hydrate. The methane molecules not captured in the cavities of the hydrate formed a single large bubble (as shown in Fig. 2), giving the MSD increasing with time (drawn as the solid line in Fig. 7b). In the presence of the amylose additive, the MSD most rapidly increased (broken line in Fig. 7b), signifying the strongest inhibition with the amylose additive.

The overall MSD of water molecules is only qualitatively related to the conversion rate of the liquid water molecules to the hydrate on the surface of the seed. As the hydrate grows, the liquid water molecules become crystalline, giving a smaller MSD of water molecules overall. The differences in the MSDs of methane with and without additive dominantly arise from capturing of methane by the hydrate cages. As can be seen in Fig. 2, methane molecules form a large bubble which does not much contact the additive. Methane molecules largely moves inside the bubble. Therefore, the spatial hindrance of the methane diffusion by the additive should be insignificant.

We examined the molecular structure of hydrate by calculating the RDFs sampled from the final portion of MD simulation (0.950–1.000 μs). Shown in Fig. 8 are the RDFs for the oxygen atoms of water, $g_{ow\text{-}ow}(r)$, and for carbon atoms of methane, $g_{cm\text{-}cm}(r)$, where r is the interatomic distance. $g_{ow\text{-}ow}(r)$ showed five peaks: three peaks located at 0.28, 0.45, and 0.68 nm arose from the liquid water. The first peak of $g_{ow\text{-}ow}(r)$ located at 0.28 nm arose from the nearest-neighboring water molecules, while the second peak at 0.45 nm originates from the local tetrahedral network of H bonds with an oxygen atom at its center [59–61]. The subsequent three peaks of $g_{ow\text{-}ow}(r)$ originated from the water molecules constituting the 5-membered and 6-membered rings of the cages of hydrate [61].

Regarding the RDFs of carbon atoms of methane, the first peak of $g_{cm\text{-}cm}(r)$ located at 0.4 nm originated from the aggregated molecules, whereas the subsequent two peaks at 0.65 and 1.05 nm correspond to the molecules separated by hydrate cages [2,62,63]. Without an additive, the first peak of $g_{cm\text{-}cm}(r)$ at 0.4 nm was shortest because the methane molecules were mainly caged by the growing hydrate. With an additive however, the first peak rose from that without an additive, signifying the molecules caged by the hydrated decreased in number

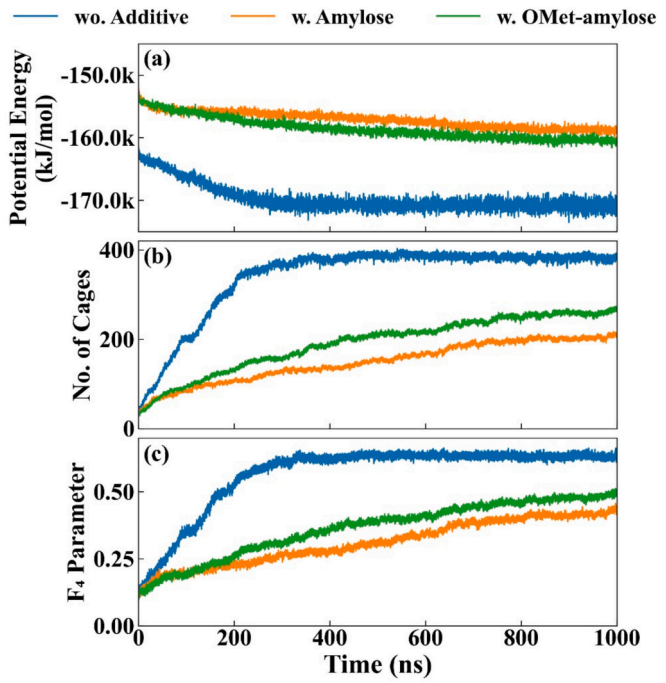


**Fig. 6.** Time evolutions of the potential energy of the system (a), the number of cages of the hydrate (b), and F4 parameter (c). Shown in blue, orange, green are the simulation results without an additive, with the amylose additive, and with the OMet-amylose additive, respectively. (For interpretation of the references to colour in this figure legend, the reader is referred to the web version of this article.)

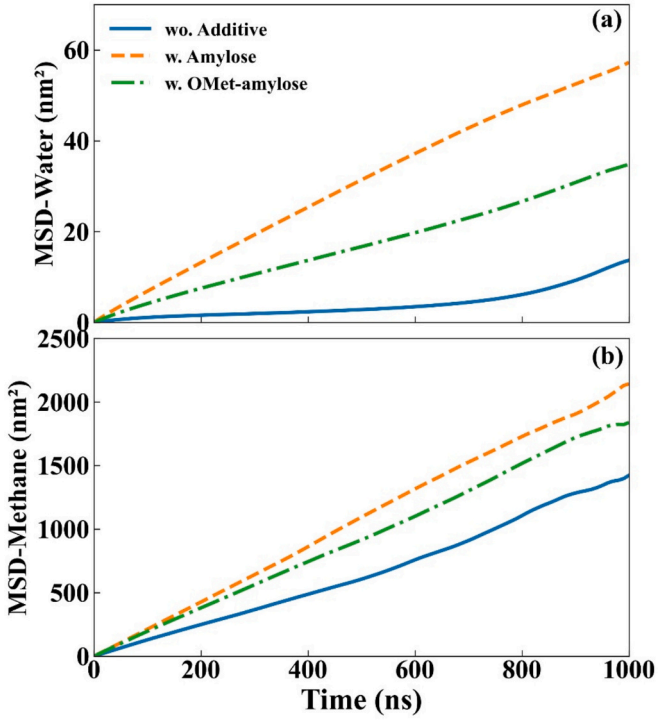


**Fig. 7.** Mean square displacements (MSDs) of the initially liquid water molecules (a) and methane molecules (b). Shown as the solid, broken, and dot-dashed lines are the MSDs for the cases without any additive, with amylose, and with OMet-amylose, respectively.

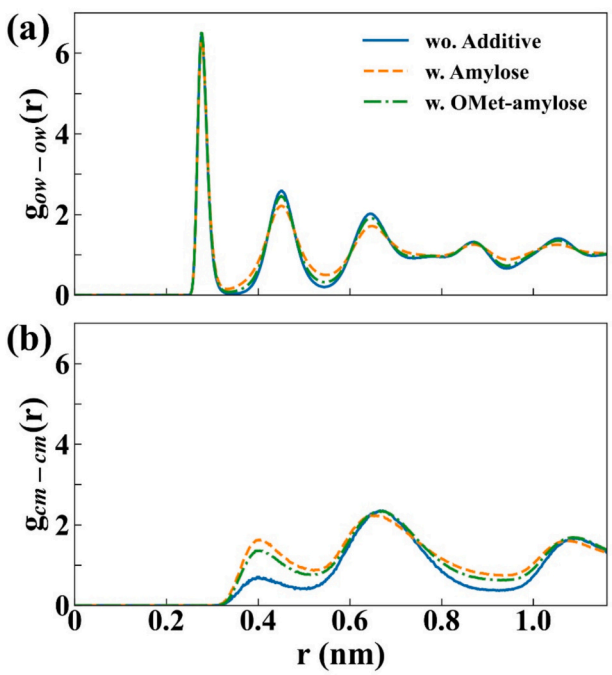


**Fig. 8.** Radial distribution functions (RDFs) for the oxygen atoms of water, $g_{ow\text{-}ow}(r)$, and for the carbon atoms of methane, $g_{cm\text{-}cm}(r)$, where r is the interatomic distance. The blue, orange, and green lines correspond to the MD simulations without any additive, with an amylose additive, and with an OMet-amylose additive, respectively. (For interpretation of the references to colour in this figure legend, the reader is referred to the web version of this article.)

with an additive. The first peak was highest with the amylose molecule, indicative of the strongest regulation of the hydrate by the amylose additive. The peaks of $g_{cm\text{-}cm}(r)$ at 0.65 nm and 1.05 nm, attributed to the methane molecules separated by hydrate cages [35,62], were similar in height regardless of the presence and identity of additive.

We enumerated the number of H bonds between the (OMet-) amylose and water molecules (Table 1). In a liquid water, the amylose molecule formed 69.58H bonds on average with the surrounding water molecules. By introducing the seed, the number decreased to 65.79 which is about 4 fewer. This originated from the ring structures formed between the hydroxyl groups of the amylose molecule and the water molecules belonging to the seed (see Fig. 4). The OMet-amylose molecule developed 43.82H bonds in the liquid water which is nearly 26 less than found for the amylose molecule. On the surface of the hydrate seed, the OMet-amylose molecule made 43.56H bonds, which is almost identical to the number in the liquid water. Therefore, the adsorption of the OMet-amylose molecule was not through the H-bond interaction.

The steric hindrances of the amylose and OMet-amylose molecules were quantified in the growth of the hydrate by calculating SASAs (Table 1). As expected, the OMet-amylose (bulkier) molecule has a SASA approximately 5 $nm^2$ larger than that of the amylose molecule (Table 1). With a larger SASA, the OMet-amylose molecule should give a steric hindrance greater than the amylose molecule. As seen above however,

**Table 1**
Number of H bonds made between the additive (amylose or OMet-amylose) molecule and water molecules. Also listed are the solvent accessible surface areas (SASAs) of additive molecules.

| System | No. of H bonds | Solvent Accessible Surface Area ($nm^2$) |
|---|---|---|
| Amylose dissolved in a liquid water | 69.58 | 19.47 |
| Amylose added to a methane hydrate | 65.79 | 19.50 |
| OMet-amylose dissolved in a liquid water | 43.82 | 24.85 |
| OMet-amylose added to a methane hydrate | 43.56 | 24.74 |

the inhibition of the hydrate by the OMet-amylose molecule was weaker than by the amylose molecule. Therefore, the H-bond interaction should be crucial in the strong regulation of hydrate by the amylose molecule.

Starch is actually a mixture of amylose and amylopectin. The present simulation focused on the structurally linear amylose. As the monomers of amylopectin and amylose are identical, the present conclusion on the role of H bond interaction in the inhibition should be valid for amylopectin as well. The branched structure of amylopectin however will give a different steric hindrance on the growing hydrate. A definitive and thorough understanding of the inhibition by amylopectin requires a future investigation.

Admittedly, simulation of the full phase transition from a liquid to a hydrate is computationally challenging and can take much longer than 1 microsecond. Herein, we did not attempt to study the full phase transition which covers the nucleation, growth, and stabilization of a gas hydrate from a liquid water. Instead, we focus on the growth of a nucleation seed for a gas hydrate. The inhibition of the growth of seed by an additive could be clearly seen within the present simulation timescale.

The low solubility and failure under high subcooling conditions are common challenges for kinetic hydrate inhibitors. This problem can be solved by using the kinetic inhibitors together with thermodynamic inhibitors. Herein, we studied the possibility of starch as a kinetic inhibitor because starch is biodegradable, non-toxic, and cost effective. Also, the present molecular insights can serve as design principles for additives chemically and structurally similar to starch.

The present condition (250 K and 100 bar) is in the range of conditions for the deep ocean (<270 K and 30 to 300 bar). As suggested, we performed additional simulations at a higher temperature 270 K (Fig. S3). We obtained results consistent with the present study: the presence of (OMet-) amylose additive significantly slowed down the growth of hydrate. The growth in the number of cages were similar up to 370 ns, presumably due to the fact that the H-bond interactions are somewhat weakened with an increased temperature. Eventually however, the growth was the slowest with the amylose additive, signifying the importance of H bond interaction in the inhibition of the additive. The present conclusions should be valid for a substantial range of temperatures and pressures.

The computational studies on the inhibition of a gas hydrate abound in the literature: MD simulation was used to study the nucleation and growth of methane hydrates with addition of phenylalanine and tryptophan [64]. The effects of lignin on the formation of methane hydrate in clay nanopores were computationally studied [34]. The present study aims at the molecular insights into the contentious role of starch which are challenging to obtain in experimental approaches. The experimental validation is beyond the scope of the present work, but, hopefully, our findings might encourage follow-up experimental investigations.

Other than the H-bond and steric hindrance, another possible origin of the differing inhibition strengths of amylose and OMet-amylose might be the difference in the molecular flexibility [65]. As shown in Fig. S4 however, both additives had similar flexibilities in that their root-mean-square fluctuations (RMSFs) on the hydrate surface were low and close to each other. Therefore, the H bond and the steric hindrance seem the main origins of the inhibition effects seen for the present additives.

## 4. Conclusions

Using all-atom MD simulation, we studied the regulation of a methane hydrate by employing an amylose (main component of starch) additive. The molecular structure and dynamics behind the regulation were studied by examining the energetic, structural, and dynamical features of the growth of a methane hydrate. With an amylose additive, the growth of a hydrate was significantly retarded. The molecular mechanism of the regulation was twofold. First, the H-bonds between the amylose molecule and the seed of hydrate. Second, the steric hindrance of the amylose molecule that prevents the liquid water molecules from contacting the seed. In the presence of another additive, OMet-amylose, which is bulkier and should give a greater steric hindrance, the regulation of hydrate was actually weaker than with the smaller amylose additive. Therefore, the H-bond interaction should be the main source of the regulation by the amylose additive. We did not find any promotion of a hydrate by the amylose additive. Presumably, any promotion effect of starch on the gas hydrate, if there is any, might come amylopectin, another major component of starch.

## CRediT authorship contribution statement

**Jaeyoung Kim:** Writing – original draft, Visualization, Software, Investigation, Conceptualization. **Seyong Choi:** Validation, Software, Investigation. **Kiduk Kim:** Visualization, Software, Investigation. **Sungwook Chung:** Writing – review & editing. **Joonkyung Jang:** Writing – review & editing, Writing – original draft, Validation, Supervision, Project administration.

## Declaration of competing interest

The authors declare the following financial interests/personal relationships which may be considered as potential competing interests: Joonkyung Jang reports financial support was provided by Korea Evaluation Institute of Industrial Technology. If there are other authors, they declare that they have no known competing financial interests or personal relationships that could have appeared to influence the work reported in this paper.

## Acknowledgements

This work was supported by the Korea Planning & Evaluation Institute of Industrial Technology and funded by the Korean Government (Ministry of Trade, Industry, and Energy, Ministry of Science and ICT, Ministry of the Interior and Safety, National Fire Agency, Project Title: Development of gas hydrate extinguishing agent and fire suppression technology for inaccessible fires, Project Number: 2760000036).

## Appendix A. Supplementary data

Supplementary data to this article can be found online at https://doi.org/10.1016/j.molliq.2025.128687.

## Data availability

Data will be made available on request.

## References

[1] E.D. Sloan Jr., Fundamental principles and applications of natural gas hydrates, Nature 426 (6964) (2003) 353–359.
[2] E.D. Sloan Jr., C.A. Koh, Clathrate hydrates of natural gases, CRC Press, 2007.
[3] J. Long, E. Sloan, Hydrates in the ocean and evidence for the location of hydrate formation, Int. J. Thermophys. 17 (1996) 1–13.
[4] J.-J. Wu, M.-Q. Kang, F.-L. Hu, et al., Comparing hydrate-based method with freezing/thawing method for chromium hydroxide sulfate removal close to the melting point of ice, Sep. Purif. Technol. 266 (2021) 118523.
[5] H. Kubota, K. Shimizu, Y. Tanaka, T. MakIta, Thermodynamic properties of R13 (CCIF3), R23 (CHF3), R152a (C2H4F2), and propane hydrates for desalination of sea water, J. Chem. Eng. Jpn. 17 (4) (1984) 423–429.
[6] K.K. Kang KyungChan, P. Linga, P.K. Park KyeongNam, C.S. Choi SangJune, L. J. Lee JuDong, Seawater desalination by gas hydrate process and removal characteristics of dissolved ions (Na+, K+, Mg2+, Ca2+, B3+, Cl-, SO42-), Desalination 353 (17) (2014) 84–90.
[7] N. Goel, In situ methane hydrate dissociation with carbon dioxide sequestration: current knowledge and issues, J. Petrol. Sci. Eng. 51 (3–4) (2006) 169–184.
[8] H.P. Veluswamy, A.J.H. Wong, P. Babu, et al., Rapid methane hydrate formation to develop a cost effective large scale energy storage system, Chem. Eng. J. 290 (2016) 161–173.
[9] I. Cha, S. Lee, J.D. Lee, G.-w. Lee, Y. Seo, Separation of SF6 from gas mixtures using gas hydrate formation, Environ. Sci. Technol. 44 (16) (2010) 6117–6122.

[10] J. Cai, C.-G. Xu, Z.-M. Xia, Z.-Y. Chen, X.-S. Li, Hydrate-based methane separation from coal mine methane gas mixture by bubbling using the scale-up equipment, Appl. Energy 204 (2017) 1526–1534.
[11] Q. Zhang, C. Li, Q. Wu, B. Zhang, Effect of dry water on methane separation and recovery from coal mine gas based on hydrate, RSC Adv. 8 (48) (2018) 27171–27180.
[12] Z. Tu, L. Li, F. Wang, Y. Zhang, Review on separation of coalbed methane by hydrate method, Fuel 358 (2024) 130224.
[13] Y.F. Makogon, Hydrates of Hydrocarbons, 1997.
[14] J.B. Klauda, S.I. Sandler, Global distribution of methane hydrate in ocean sediment, Energy Fuel 19 (2) (2005) 459–470.
[15] Y. Song, L. Yang, M. Yang, Natural gas hydrate, far beyond a vast resource of natural gas: the innovation, Innov. Energy 2 (2) (2025) 100074.
[16] S.-P. Kang, H. Lee, Recovery of CO2 from flue gas using gas hydrate: thermodynamic verification through phase equilibrium measurements, Environ. Sci. Technol. 34 (20) (2000) 4397–4400.
[17] H. Wang, L. Zhang, J. He, T. Zhou, The development of natural gas hydrate exploitation technology from perspective of patents, Front. Energy Res. 10 (2022) 860591.
[18] M.A. Kelland, History of the development of low dosage hydrate inhibitors, Energy Fuel 20 (3) (2006) 825–847.
[19] E. Hammerschmidt, Formation of gas hydrates in natural gas transmission lines, Ind. Eng. Chem. 26 (8) (1934) 851–855.
[20] E.D. Sloan, Natural Gas Hydrates in Flow Assurance, Gulf Professional Publishing, 2010.
[21] A. Perrin, O.M. Musa, J.W. Steed, The chemistry of low dosage clathrate hydrate inhibitors, Chem. Soc. Rev. 42 (5) (2013) 1996–2015.
[22] J.D. Lee, H. Wu, P. Englezos, Cationic starches as gas hydrate kinetic inhibitors, Chem. Eng. Sci. 62 (23) (2007) 6548–6555.
[23] C.A. Koh, Towards a fundamental understanding of natural gas hydrates, Chem. Soc. Rev. 31 (3) (2002) 157–167.
[24] Innovative KHI polymers for gas hydrate control, in: Offshore Technology Conference, OTC, 2011.
[25] L.D. Villano, R. Kommedal, M.W. Fijten, U.S. Schubert, R. Hoogenboom, M. A. Kelland, A study of the kinetic hydrate inhibitor performance and seawater biodegradability of a series of poly (2-alkyl-2-oxazoline) s, Energy Fuel 23 (7) (2009) 3665–3673.
[26] A. Singh, A. Suri, Enhanced hydrate inhibition by plant-based polysaccharides as synergists with kinetic hydrate inhibitors, Energy Fuel 36 (13) (2022) 6974–6988.
[27] A.V. Fakhreeva, V.V. Nosov, A.I. Voloshin, V.A. Dokichev, Polysaccharides are effective inhibitors of natural gas hydrate formation, Polymers 15 (7) (2023) 1789.
[28] S. Xu, S. Fan, S. Fang, X. Lang, Y. Wang, J. Chen, Pectin as an extraordinary natural kinetic hydrate inhibitor, Sci. Rep. 6 (1) (2016) 23220.
[29] M.R. Talaghat, Enhancement of the performance of modified starch as a kinetic hydrate inhibitor in the presence of polyoxides for simple gas hydrate formation in a flow mini-loop apparatus, J. Nat. Gas Sci. Eng. 18 (2014) 7–12.
[30] N. Li, X. Dong, J. Xu, et al., Influence of polyvinylpyrrolidone and cassava starch on the formation kinetics of CO2 hydrate, Energy Fuel 39 (16) (2025) 7766–7780.
[31] H. Fakharian, H. Ganji, A.N. Far, M. Kameli, Potato starch as methane hydrate promoter, Fuel 94 (2012) 356–360.
[32] S.M. Babakhani, A. Alamdari, Effect of maize starch on methane hydrate formation/dissociation rates and stability, J. Nat. Gas Sci. Eng. 26 (2015) 1–5.
[33] W. Go, S. Yun, D. Lee, Y. Seo, Dipeptides as environmentally friendly CH4 hydrate inhibitors: experimental and computational approaches, Fuel 329 (2022) 125479.
[34] M. Fengyi, H. Zhongjin, J. Guosheng, N. Fulong, Molecular insights into the effects of lignin on methane hydrate formation in clay nanopores, Energy 276 (2023) 127496.
[35] P. Xu, X. Lang, S. Fan, Y. Wang, J. Chen, Molecular dynamics simulation of methane hydrate growth in the presence of the natural product pectin, J. Phys. Chem. C 120 (10) (2016) 5392–5397.
[36] N. Zhang, Y.-T. Du, P.-Q. Yao, et al., Synergistic effect of hyperactive antifreeze protein on inhibition of gas-hydrate growth by hydrophobic and hydrophilic groups, J. Phys. Chem. B. 127 (49) (2023) 10469–10477.
[37] M. Maddah, M. Maddah, K. Peyvandi, The influence of a type III antifreeze protein and its mutants on methane hydrate adsorption–inhibition: a molecular dynamics simulation study, Phys. Chem. Chem. Phys. 21 (39) (2019) 21836–21846.
[38] J. McMurry, Organic Chemistry, OpenStax, 2023.
[39] Y. Ai, J.-l. Jane, Understanding starch structure and functionality, in: Starch in food, Elsevier, 2024, pp. 55–77.
[40] A. Lenz, L. Ojamäe, Structures of the I-, II-and H-methane clathrates and the ice-methane clathrate phase transition from quantum-chemical modeling with force-field thermal corrections, Chem. A Eur. J. 115 (23) (2011) 6169–6176.
[41] J. Abascal, E. Sanz, R. García Fernández, C. Vega, A potential model for the study of ices and amorphous water: TIP4P/Ice, J. Chem. Phys. 122 (23) (2005).
[42] T. Darden, D. York, L. Pedersen, Particle mesh Ewald: an N log (N) method for Ewald sums in large systems, J. Chem. Phys. 98 (1993) 10089–10092.
[43] R.W. Hockney, S. Goel, J. Eastwood, Quiet high-resolution computer models of a plasma, J. Comput. Phys. 14 (2) (1974) 148–158.
[44] B. Hess, H. Bekker, H.J. Berendsen, J.G. Fraaije, LINCS: A linear constraint solver for molecular simulations, J. Comput. Chem. 18 (12) (1997) 1463–1472.
[45] S. Nosé, A unified formulation of the constant temperature molecular dynamics methods, J. Chem. Phys. 81 (1) (1984) 511–519.
[46] S. Nosé, M.L. Klein, Constant pressure molecular dynamics for molecular systems, Mol. Phys. 50 (5) (1983) 1055–1076.
[47] M. Parrinello, A. Rahman, Polymorphic transitions in single crystals: a new molecular dynamics method, J. Appl. Phys. 52 (12) (1981) 7182–7190.
[48] K.N. Kirschner, A.B. Yongye, S.M. Tschampel, et al., GLYCAM06: a generalizable biomolecular force field. Carbohydrates, J. Comput. Chem. 29 (4) (2008) 622–655.
[49] W.L. Jorgensen, D.S. Maxwell, J. Tirado-Rives, Development and testing of the OPLS all-atom force field on conformational energetics and properties of organic liquids, J. Am. Chem. Soc. 118 (45) (1996) 11225–11236.
[50] W. Damm, A. Frontera, J. Tirado-Rives, W.L. Jorgensen, OPLS all-atom force field for carbohydrates, J. Comput. Chem. 18 (16) (1997) 1955–1970.
[51] H.J. Berendsen, D. van der Spoel, R. van Drunen, GROMACS: a message-passing parallel molecular dynamics implementation, Comput. Phys. Commun. 91 (1–3) (1995) 43–56.
[52] D. Van Der Spoel, E. Lindahl, B. Hess, G. Groenhof, A.E. Mark, H.J. Berendsen, GROMACS: fast, flexible, and free, J. Comput. Chem. 26 (16) (2005) 1701–1718.
[53] S. Jo, T. Kim, V.G. Iyer, W. Im, CHARMM-GUI: a web-based graphical user interface for CHARMM, J. Comput. Chem. 29 (11) (2008) 1859–1865.
[54] S.-J. Park, J. Lee, Y. Qi, et al., CHARMM-GUI Glycan Modeler for modeling and simulation of carbohydrates and glycoconjugates, Glycobiology 29 (4) (2019) 320–331.
[55] Y. Liu, K. Xu, Y. Xu, J. Liu, J. Wu, Z. Zhang, HTR: an ultra-high speed algorithm for cage recognition of clathrate hydrates, Nanotechnol. Rev. 11 (1) (2022) 699–711.
[56] P. Rodger, T. Forester, W. Smith, Simulations of the methane hydrate/methane gas interface near hydrate forming conditions conditions, Fluid Phase Equilib. 116 (1–2) (1996) 326–332.
[57] W. Humphrey, A. Dalke, K. Schulten, VMD: visual molecular dynamics, J. Mol. Graph. 14 (1) (1996) 33–38.
[58] Ł. Baran, W. Rżysko, L.G. MacDowell, Self-diffusion and shear viscosity for the TIP4P/Ice water model, J. Chem. Phys. 158 (6) (2023).
[59] T. Head-Gordon, M.E. Johnson, Tetrahedral structure or chains for liquid water, Proc. Natl. Acad. Sci. 103 (21) (2006) 7973–7977.
[60] N. Galamba, Water's structure around hydrophobic solutes and the iceberg model, J. Phys. Chem. B. 117 (7) (2013) 2153–2159.
[61] Z. Li, F. Jiang, H. Qin, B. Liu, C. Sun, G. Chen, Molecular dynamics method to simulate the process of hydrate growth in the presence/absence of KHIs, Chem. Eng. Sci. 164 (2017) 307–312.
[62] C. Moon, P.C. Taylor, P.M. Rodger, Molecular dynamics study of gas hydrate formation, J. Am. Chem. Soc. 125 (16) (2003) 4706–4707.
[63] B. Song, V. Molinero, Thermodynamic and structural signatures of water-driven methane-methane attraction in coarse-grained mW water, J. Chem. Phys. 139 (5) (2013).
[64] S. Rawat, C. Ramachandran, The nucleation and growth of methane hydrates in the presence of phenylalanine and tryptophan: a comparative molecular dynamics simulation study, Phys. Chem. Chem. Phys. 27 (20) (2025) 10591–10605.
[65] H. Yu, M. Amann, T. Hansson, J. Köhler, G. Wich, W.F. van Gunsteren, Effect of methylation on the stability and solvation free energy of amylose and cellulose fragments: a molecular dynamics study, Carbohydr. Res. 339 (10) (2004) 1697–1709.